Nuclear Materials and Energy 26 (2021) 100909

Contents lists available at ScienceDirect

Nuclear Materials and Energy

journal homepage: www.elsevier.com/locate/nme

Modelling of hydrogen atoms reflection from an annealed tungsten fuzzy surfaces

D.H. Liu [a], S.Y. Dai [a,b,*], M. Wada [c], K.R. Yang [a], J.Y. Chen [a], D.P. Liu [d], N. Cherenda [e], D. Z. Wang [a,*]

[a] Key Laboratory of Materials Modification by Laser, Ion and Electron Beams (Ministry of Education), School of Physics, Dalian University of Technology, Dalian 116024, People's Republic of China
[b] DUT-BSU Joint Institute, Dalian University of Technology, Dalian 116024, People's Republic of China
[c] Graduate School of Science and Engineering, Doshisha University, Kyotanabe, Kyoto 610-0394, Japan
[d] School of Electrical Engineering, Dalian University of Technology, Dalian 116024, People's Republic of China
[e] Department of Solid State Physics, Physics Faculty, Belarusian State University, Belarus

ARTICLE INFO

Keywords:
Tungsten
Fuzz
Porosity
Kinetic Monte Carlo

ABSTRACT

Modelling of the hydrogen reflection on tungsten smooth and fuzz surfaces under the low-energy hydrogen plasma bombardment has been performed with the three-dimensional kinetic Monte Carlo code SURO-FUZZ. The relative reflection coefficient of hydrogen atoms, i.e. the ratio of reflected hydrogen atoms on the tungsten fuzz surface to that on the tungsten smooth one, is employed to illustrate the change in the hydrogen reflection on the tungsten fuzz and smooth surfaces. The simulated relative reflection coefficient of hydrogen atoms shows a large discrepancy with the measured values obtained in the hydrogen plasma bombardment experiment. The impinging hydrogen particles with a low incident energy result in a small sputtering and large residual nanostructure existing on the tungsten fuzz surface, which lead to a small change in the relative reflection coefficient of hydrogen atoms. The discrepancy between simulations and experiments motivates us to take the impacts of the annealing effect into account in SURO-FUZZ code. Implementation of annealing effect into SURO-FUZZ has been benchmarked against the experimental data. The simulated temporal evolution of the hydrogen reflection coefficient is in reasonable agreement with the experimental data.

1. Introduction

Tungsten is a candidate material for plasma-facing components of fusion devices like ITER owing to its high melting point and thermal conductivity, low sputtering yield and hydrogen isotopes retention [1]. However, experiments performed in linear and tokamak devices with helium-containing plasma observed that a fiber-form nanostructure called "fuzz", which consists of numerous nanoscale tendrils, is formed on the tungsten surface [2–7]. The formation of the tungsten fuzz can decrease the fuel retention and the secondary electron emission yield, and resist surface cracking under transient plasma loads [8–14]. On the other hand, it strongly reduces the thermal conductivity and the optical reflectivity, and easily triggers unipolar arcing [15–19]. Therefore, studies on the fuzz property are essential for tungsten divertor lifetime and steady-state operation [19–22].

The reflection property of particle plays an important role in fuel recycling, edge plasma parameters and even steady-state operation. Recent experiments related to the particle reflection on the tungsten fuzz surface have been performed on a linear device. The definition of the relative reflection coefficient of hydrogen atoms is introduced to characterize the change of the hydrogen reflection, which is the ratio of reflected hydrogen atoms on the tungsten fuzz surface to that on the tungsten smooth one. The prepared tungsten fuzz nanostructure is destroyed under the hydrogen plasma bombardment, meanwhile the relative reflection coefficients of hydrogen atoms increase and finally saturate with exposure time. Hence, the results indicate that the destruction of the tungsten fuzz nanostructure causes the increase of the relative reflection coefficients of hydrogen atoms [23,24].

The impacts of incident energy on the relative reflection coefficient of hydrogen atoms have been studied in the above-mentioned

* Corresponding authors at: Key Laboratory of Materials Modification by Laser, Ion and Electron Beams (Ministry of Education), School of Physics, Dalian University of Technology, Dalian 116024, People's Republic of China (S.Y. Dai).
E-mail addresses: daishuyu@dlut.edu.cn (S.Y. Dai), wangdez@dlut.edu.cn (D.Z. Wang).

https://doi.org/10.1016/j.nme.2021.100909
Received 20 November 2020; Received in revised form 6 January 2021; Accepted 7 January 2021
Available online 21 January 2021

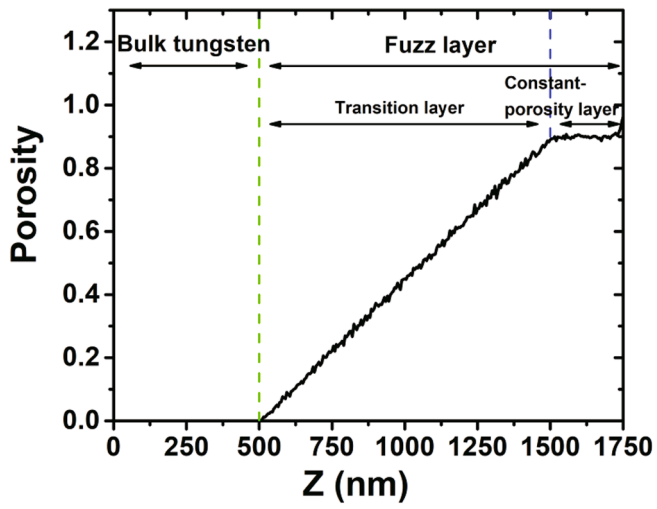

Fig. 1. Profiles of the porosity as a function of the tungsten fuzz nanostructure height.

experiments [23]. It is found that the low incident energy of hydrogen particles results in a small relative reflection coefficient of hydrogen atoms in comparison to the high incident energy. In our previous work, the modelling of the relative reflection coefficient of hydrogen atoms for the case of the high incident energy shows a good agreement with the measured value [25]. In this work, the simulations have been attempted by the three-dimensional (3D) SURO-FUZZ code to reproduce the measured relative reflection coefficient of hydrogen atoms for the case of low incident energy. However, the simulation results show a large discrepancy with the measurements due to the low sputtering yield of tungsten fuzz surface. The small sputtering yield is not sufficient to destroy the tungsten fuzz nanostructure. The recent experiments revealed that the nanostructure can be annealed out at elevated temperatures [26–29]. Hence, the update of SURO-FUZZ code has been performed to include the annealing effect. Based on this upgrade, a reasonable agreement between the simulations and measurements can be achieved in the relative reflection coefficient of hydrogen atoms for the low incident energy. The current work is organized as follows: a detailed description of the SURO-FUZZ model is provided in Section 2. The effects of the physical sputtering and annealing effects are discussed in Sections 3.1 and 3.2, respectively. Finally, the summary is presented in Section 4.

2. Simulation model

The SURO-FUZZ code, which was developed based on 3D rough surface code SURO [30–33], has been applied to study the relative reflection coefficient of hydrogen atoms [25]. The distributions of the porosity against height have been measured on NAGDIS-II device (Fig. 9 (b) in [26]). The porosity on the surface of fuzz is principally constant around 0.9 and it decreases virtually linearly from the top to the bulk. Based on this measured porosity distribution, the tungsten fuzz

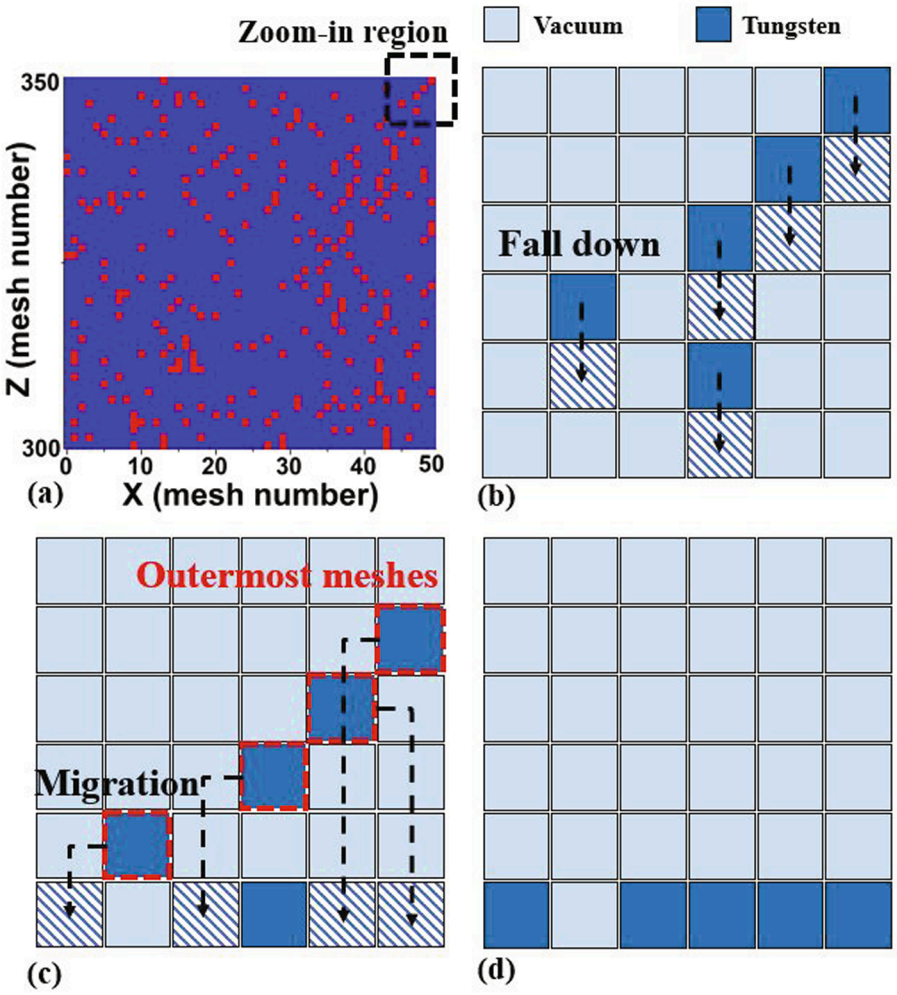

Fig. 2. The schematic view of the simple and improved annealing models. (a) The cross sections of the top region of the initially constructed fuzz nanostructure. (b) and (c) are the schematic views of the simple annealing model and the improved annealing model, respectively. The light blue, dark blue, shaded meshes represent vacuum, tungsten, the newly migrated tungsten meshes. Tungsten meshes with the red dashed lines are the outermost tungsten meshes. (d) The resultant tungsten mesh positions for the improved annealing model. (For interpretation of the references to colour in this figure legend, the reader is referred to the web version of this article.)

nanostructure in SURO-FUZZ model has been divided into three sub-layers (the tungsten bulk, transition and constant-porosity layers) to describe the porosity distribution in the porous tungsten nanostructure. Fig. 1 shows the profile of the porosity of the initial tungsten fuzz nanostructure as a function of height, and the initial porosity distribution in each layer can be described by the following formulae:

$$\rho(Z) = \begin{cases} \rho_0 & Z_{trans} < Z < Z_{constant} \quad (constant\ -\ porosity\ layer) \\ \dfrac{Z - Z_0}{Z_{trans} - Z_0} \times \rho_0 & Z_0 < Z < Z_{trans} \quad (transition\ layer) \\ 0 & 0 < Z < Z_0 \quad (bulk\ tungsten) \end{cases} \tag{1}$$

where ρ_0 is the pre-defined porosity in the constant-porosity layer and $\rho(Z)$ is the porosity at each height, $Z_{constant}$, Z_{trans} and Z_0 are the heights of the constant-porosity layer, transition layer and bulk, respectively. Here, $\rho_0 = 0.9$, $Z_{constant} = 1750$ nm, $Z_{trans} = 1500$ nm and $Z_0 = 500$ nm are used, which are the same as our previous work [25]. The simulation box is composed of $50 \times 50 \times 500$ volumetric meshes, and each mesh has a size of $5 \times 5 \times 5$ nm^3. Based on the porosity distribution, the tungsten fuzzy structure can be built up by means of the Monte Carlo method. A uniform random number *rand* is employed to compare with the porosity $\rho(Z)$ at each position. When *rand* is higher than $\rho(Z)$, a tungsten mesh is created, otherwise, a vacuum mesh is created.

After the tungsten fuzz nanostructure is initially established, and the bombardment of the nanostructure by incident particles can be triggered. The input information of impinging particles for SURO-FUZZ simulations (flux, angle and energy) is calculated by SDPIC code [34–36]. The incident particles are emitted from the top boundary ($Z =$ 2500 nm) and move along the direction provided by SDPIC. The volumetric meshes are described by the cubic cells in the SURO-FUZZ model. The local surface normal vector is perpendicular to each surface of cubic cells. When the incident particles reach the surface, the local angle is calculated according to the incident direction and the local surface normal at the impact position. Then the incident particles implant into the tungsten substrate or reflect from the tungsten surface. The reflection probability of the incident particles is calculated by the TRIM code [37]. The reflected hydrogen atoms that leave the top boundary are used to calculate the relative reflection coefficient of hydrogen atoms. The physical sputtering of tungsten fuzz nanostructure has been taken into account, which is calculated by the empirical formulae in Ref. [38].

The recent experiments revealed that the thickness of the fuzz layer can be annealed out at elevated temperatures [26–29]. Hence, an annealing module has been developed and implemented into SURO-FUZZ code, which describes the reintegrated process of the agglomerated tungsten nanostructure. The annealing process of the tungsten fuzz nanostructure shows a dependence on the annealing time in the experiments [26]. Accordingly, in the modelling, the time interval ($t_{annealing}$) is employed as a controlling parameter to treat the degradation of the tungsten fuzz nanostructure. Two approaches (simple annealing model and improved annealing model) are proposed to simulate the falling process of tungsten meshes due to the annealing effect. The movement of the tungsten meshes during the annealing process can be described as shown in Fig. 2. The cross section of the top region of the initially constructed fuzz nanostructure is shown in Fig. 2(a). The region labeled by the dashed black square (denominated as zoom-in region) in Fig. 2(a) is selected in order to explain the migration of tungsten meshes as shown in Fig. 2(b–d). The schematics in Fig. 2(b–d) correspond to the zoom-in region in Fig. 2(a). The light blue, dark blue and shaded meshes in Fig. 2 (b–d) represent vacuum, tungsten meshes and the newly migrated tungsten meshes, respectively.

In the simple annealing model, the tungsten meshes in the constant-porosity and transition layers drop one-mesh height along the vertical direction every $t_{annealing}$ when the below mesh is a vacuum mesh, which is shown schematically in Fig. 2(b). The shaded meshes in Fig. 2(b) represent the new position after the falling down of the tungsten meshes. In the improved annealing model, after the vertical falling of tungsten meshes in the above-mentioned simple annealing model, the outermost tungsten meshes (tungsten meshes with red dashed lines) would be migrated (named as the migrated meshes) as shown in Fig. 2(c). Here, the outermost tungsten meshes are referred to as the highest tungsten cells in a certain X and Y coordinate. The approach for tungsten mesh migration is treated as follows: The migrated mesh and its eight adjacent outermost tungsten meshes (nine meshes in total) are selected to deal with the movement of the migrated mesh. The height of the migrated mesh will be compared with the eight adjacent outermost tungsten meshes. If the migrated mesh is not the lowest mesh for all nine outermost tungsten meshes, the migrated mesh will drop onto the lowest adjacent outermost tungsten mesh. If the migrated mesh is lower than the eight adjacent outermost tungsten meshes, the migrated mesh will drop along the vertical direction. The resultant tungsten mesh positions for the improved annealing model are sketchily shown in Fig. 2(d).

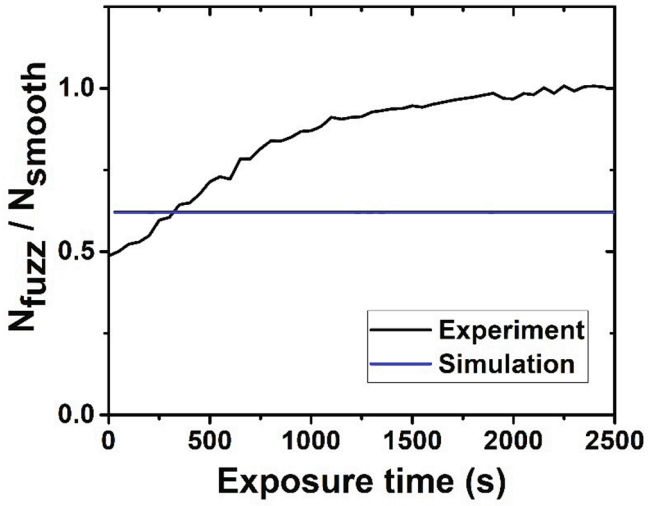

Fig. 3. The temporal evolution of hydrogen relative reflection coefficients of hydrogen atoms.

3. Results and discussion

3.1. Comparison between experiment and simulation

In the hydrogen plasma bombardment experiment, the hydrogen plasma irradiates the prepared tungsten fuzz surface and tungsten smooth surface, respectively. The electron density and the temperature are estimated to be $n_e = 4 \times 10^{11}$ cm^{-3} and $T_e = 3.0$ eV. The magnetic field strength is 28 mT, which is inclined of 45° with respect to the normal to the sample surface. The sample surface is biased with the potentials of $V_b = -300$, -250 and -200 V [23]. In this work, the case with a low incident energy (corresponding to $V_b = -200$ V) is studied.

The incident flux, angle and energy of hydrogen plasma are calculated by SDPIC code according to the above-mentioned experiment parameters. The calculated incident flux is about 5.0×10^{21} m^{-2} s^{-1}. Since the majority of the incident particles is H_2^+ ions and the minority is H^+ ions in the experiment, the incident fluxes of H^+ and H_2^+ ions are assumed to be 1.0×10^{21} and 4.0×10^{21} m^{-2} s^{-1}, respectively. The calculated incident angle of hydrogen particles is around 10° and the calculated incident energy is about 230 eV for $V_b = -200$ V. The above incident particle information (flux, angle and energy) obtained by SDPIC simulation are employed as input for the following SURO-FUZZ modelling.

The threshold energies of physical sputtering for the H^+ and H_2^+ ions impinging the tungsten surface are about 458 and 214 eV, respectively.

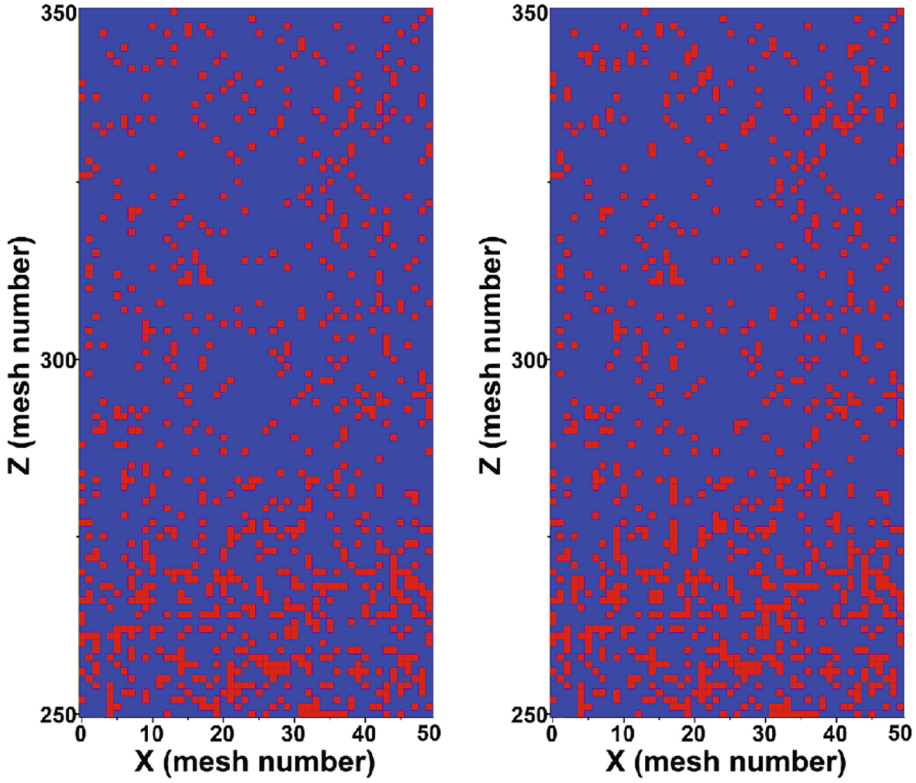

Fig. 4. Cross sections of the tungsten fuzz surface at 0 s (a) and 2500 s (b).

In the experiment, the measured H atom reflection coefficients are derived from the H atoms caused by the energetic H^+ ions, which can be distinguished from the H atoms with a low energy from diffusion and H atoms derived from the energetic H_2^+ ions by using the Doppler-broadened profile [23]. The reflected H atoms of the energetic incident H^+ ions can return to the background plasma, which is utilized to calculate the reflection coefficients.

Fig. 3 shows the time evolution of the relative reflection coefficients of hydrogen atoms (N_{fuzz}/N_{smooth}) by the SURO-FUZZ modelling (without the annealing effect). Here, N_{fuzz} and N_{smooth} represent the number of H atoms reflected from the tungsten fuzz and smooth surfaces, respectively. The incident H^+ ions can undergo more reflections at the rough fuzz surface with a high porosity, which can prevent the reflected H atoms escaping from the tungsten surface. Therefore, the initial hydrogen reflection coefficient on the tungsten fuzz surface is 50% lower than that on the smooth one in the experiment. As the exposure time increases, the tungsten fuzz nanostructure is destructed gradually, which can mitigate the hydrogen trapping effect of the tungsten fuzz surface on the reflected H atoms. As a result, the measured relative reflection coefficient of hydrogen atoms in the experiment (as shown in black curve of Fig. 3) increases gradually with the destruction of the porous tungsten fuzz nanostructure. However, it is found that the relative reflection coefficient of hydrogen atoms in the modelling (as shown in blue curve of Fig. 3) is almost constant.

Fig. 4 shows that cross sections of the initial fuzz nanostructure and the fuzz nanostructure after 2500 s exposure in the modelling, respectively. The red and blue meshes are tungsten and vacuum meshes, respectively. It can be seen that the heights of the fuzz nanostructure in Fig. 4(a) and (b) are almost identical. This indicates that the physical sputtering is too low to destroy the nanostructure on the fuzz surface, which results in the nearly constant relative reflection coefficient of hydrogen atoms as shown in Fig. 3. Since the incident energy of H^+ ions (230 eV) is less than H^+ ions sputtering threshold energy (458 eV), there is no physical sputtering induced by H^+ ions. While for incident H_2^+ ions, the incident energy (230 eV) is a little higher than H_2^+ ions threshold

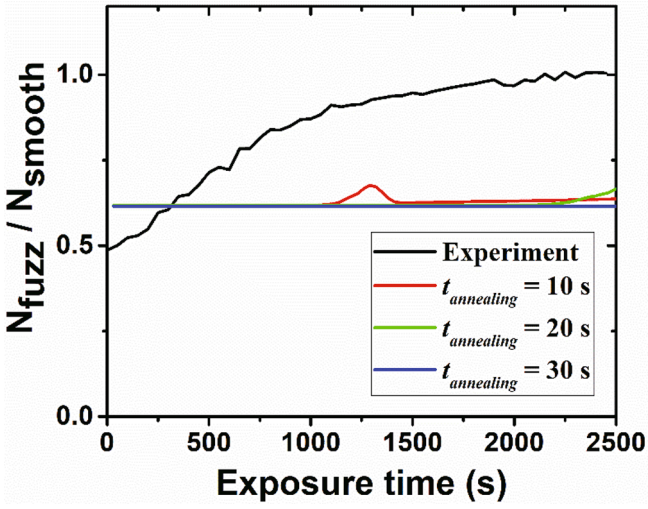

Fig. 5. The temporal evolution of the relative reflection coefficients of hydrogen atoms by the simple annealing model and experimental measurements.

energy (214 eV). The corresponding physical sputtering yield for H_2^+ ions is about 10^{-6} at 230 eV, which is too low to destroy the tungsten fuzz nanostructure. As a result, the relative reflection coefficient of hydrogen atoms has a negligible change against the exposure time in Fig. 3. The above simulation results indicate that the effect of the physical sputtering is not sufficient to interpret the experimental results. The resolidification of the agglomerated nanostructures has been observed on the surface as shown in Fig. 1(d) of Ref. [23], which is likely induced by the annealing effect. Hence, the annealing effect is studied in the following subsection to check its impact on the evolution of the relative reflection coefficients of hydrogen atoms.

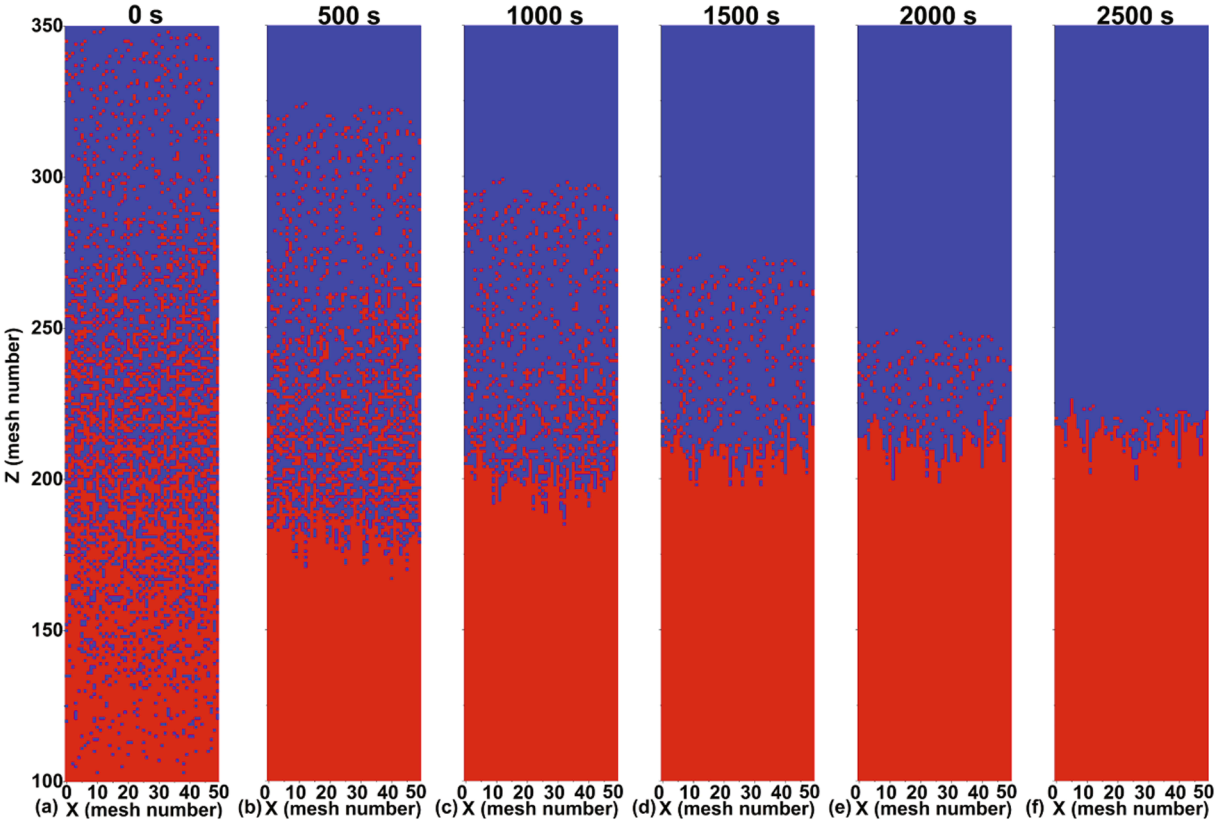

Fig. 6. Cross sections of the tungsten fuzz surface with the simple annealing model at the exposure timings of 0, 500, 1000, 1500, 2000 and 2500 s, respectively ($t_{annealing}$ = 20 s).

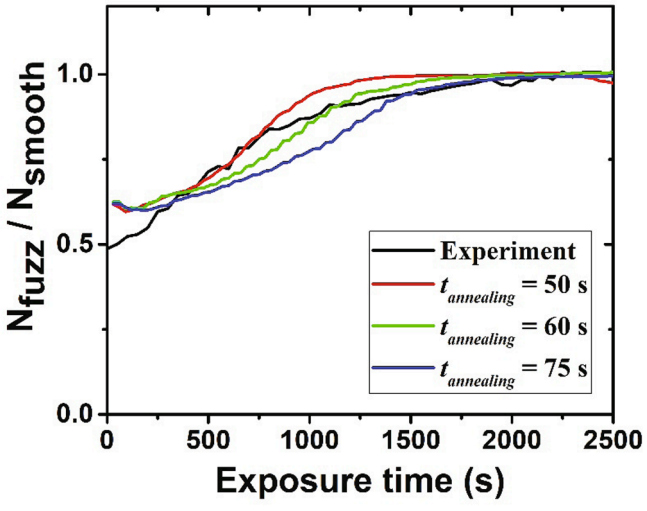

Fig. 7. The temporal evolution of the relative reflection coefficients of hydrogen atoms by the improved annealing model and experimental measurements.

3.2. Simulation with annealing effect

Fig. 5 shows the time evolution of the relative reflection coefficients of hydrogen atoms by the simple annealing model and experimental measurements. The annealing time intervals $t_{annealing}$ = 10, 20 and 30 s are used in the simulations. In order to illustrate the change of the tungsten fuzz nanostructure, cross sections of the fuzz nanostructure for exposure timings of 0, 500, 1000, 1500, 2000 and 2500 s are shown in Fig. 6 for $t_{annealing}$ = 20 s. The height of the tungsten nanostructure is referred to as the highest height of the tungsten meshes in the cross section. The height of the initial tungsten nanostructure is 1750 nm before the hydrogen plasma bombardment. The heights of the tungsten nanostructure are decreased to 1615, 1500, 1370, 1250 and 1130 nm for exposure time of 500, 1000, 1500, 2000 and 2500 s, respectively.

Despite the decrease in height, it has been checked that the porosities at the top of the tungsten surface are almost same in Fig. 6(a–e). The previous works demonstrated that the relative reflection coefficient of hydrogen atoms is dependent on the porosity at the top of the tungsten surface [25]. Hence, the almost unchanged porosity in Fig. 6(a–e) results in the small variation of the relative reflection coefficient of hydrogen atoms before 2200 s. The porosity at the top of the tungsten surface is slightly reduced after 2200 s in Fig. 6(e, f), meanwhile the relative reflection coefficient of hydrogen atoms increases marginally in green curves of Fig. 5. Therefore, the simulation results of the relative reflection coefficient of hydrogen atoms shows a large discrepancy with the experimental measurements as shown in green curves of Fig. 5.

Fig. 7 shows the time evolution of the relative reflection coefficients of hydrogen atoms by the improved annealing model and experimental measurements. The annealing time intervals $t_{annealing}$ = 50, 60 and 75 s are used in the modelling. As is seen that the simulated relative reflection coefficient of hydrogen atoms shows a reasonable agreement with the measured values for $t_{annealing}$ = 60 s. Fig. 8 shows cross sections of the fuzz nanostructure for $t_{annealing}$ = 60 s. The heights of the tungsten nanostructure are decreased to 1565, 1465, 1370, 1280 and 1215 nm for exposure times of 500, 1000, 1500, 2000 and 2500 s, respectively. The porosity at the top of the fuzz surface significantly reduces before 1500 s, which leads to a strong increase in the relative reflection coefficient of hydrogen atoms before 1500 s as shown in green curves of Fig. 7. As the exposure time increases, the fuzz surface becomes smooth as shown in Fig. 8(d–f), which results in a virtually same relative reflection coefficient of hydrogen atoms for both simulations and experiments.

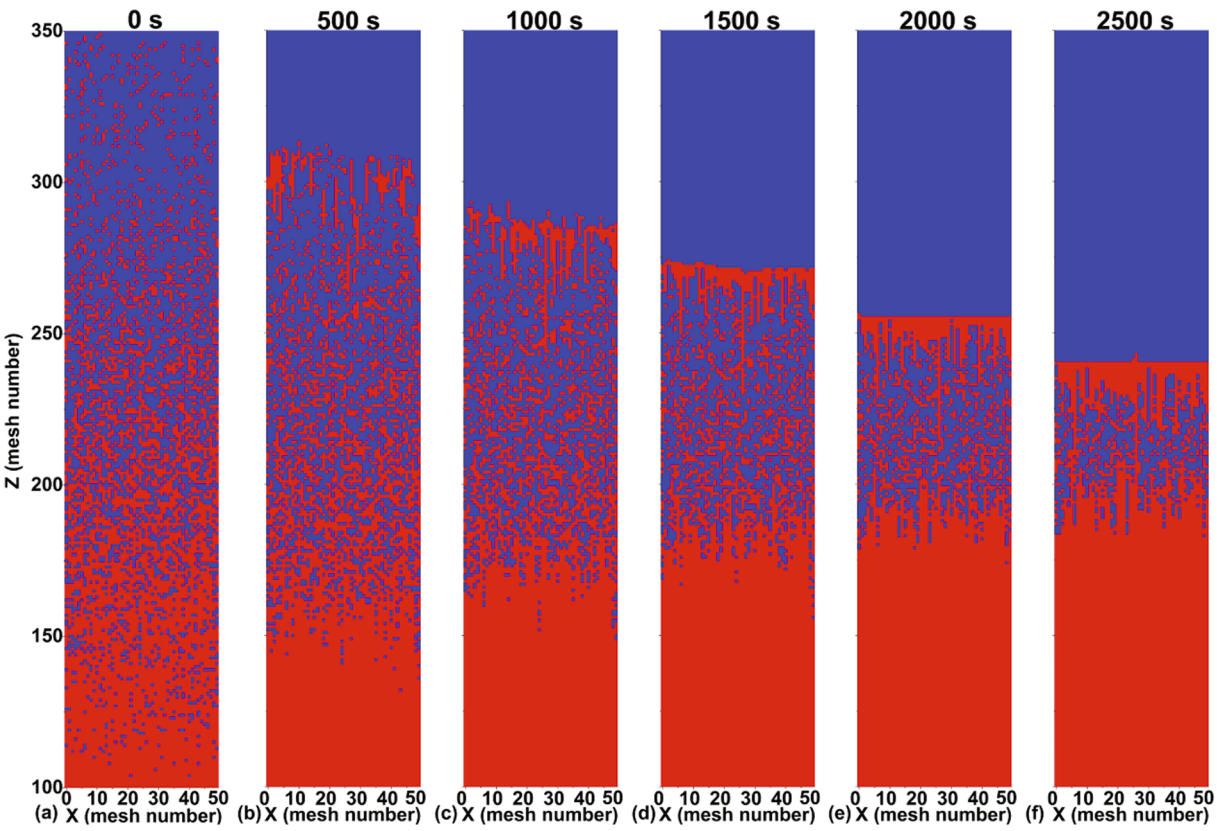

Fig. 8. Cross sections of the tungsten fuzz surface with the improved annealing model at the exposure timings of at 0, 500, 1000, 1500, 2000 and 2500 s, respectively ($t_{annealing}$ = 60 s).

4. Summary

Simulations of the hydrogen reflection on tungsten smooth and fuzz surfaces under the low-energy hydrogen plasma bombardment have been performed by SURO-FUZZ code. The low incident energy of hydrogen particles causes a small physical sputtering yield, which is not sufficient to destroy the tungsten fuzz structure. The undestroyed fuzz nanostructures trap the hydrogen atoms, which leads to a small reflection of hydrogen atoms. Hence, the simulated relative reflection coefficient of hydrogen atoms shows a large discrepancy with the measured values.

A new development of the annealing module (simple annealing and improved annealing models) has been implemented into SURO-FUZZ. In the simple annealing model, the relative reflection coefficient of hydrogen atoms is almost constant although the height of the tungsten nanostructure decreases, which is still different from the measurements. In the improved annealing model, besides the height of the tungsten nanostructure decreases, the outermost layer of tungsten nanostructure becomes smooth with exposure time. The simulated temporal evolution of the hydrogen reflection coefficient is in reasonable agreement with the experimental data.

CRediT authorship contribution statement

D.H. Liu: Conceptualization, Software, Writing - original draft. **S.Y. Dai:** Formal analysis, Writing - review & editing, Supervision. **M. Wada:** Resources, Investigation. **K.R. Yang:** Writing - review & editing. **J.Y. Chen:** Writing - review & editing. **D.P. Liu:** Writing - review & editing, Visualization. **N. Cherenda:** Writing - review & editing, Methodology. **D.Z. Wang:** Funding acquisition, Project administration.

Declaration of Competing Interest

The authors declare that they have no known competing financial interests or personal relationships that could have appeared to influence the work reported in this paper.

Acknowledgments

This work was supported by National MCF Energy R&D Program of China Nos. 2018YFE0303105, 2017YFE0301206 and 2018YFE0311100, National Natural Science Foundation of China under Grant No. 12075047 and High-level talent innovation support program of Dalian No. 2017RQ052.

References

[1] R.A. Pitts, et al., J. Nucl. Mater. 438 (2013) S48.
[2] S. Takamura, et al., Plasma Fusion Res. 1 (2006) 51.
[3] M.J. Baldwin, et al., Nucl. Fusion 48 (2008), 035001.
[4] S. Kajita, et al., Nucl. Fusion 49 (2009), 095005.
[5] S. Kajita, et al., J. Nucl. Mater. 418 (2011) 152.
[6] Y. Ueda, et al., J. Nucl. Mater. 415 (2011) S92.
[7] G.M. Wright, et al., Nucl. Fusion 52 (2012), 042003.
[8] D. Nishijima, et al., J. Nucl. Mater. 415 (2011) S96.
[9] D. Nishijima, et al., Fusion Sci. Technol. 60 (2011) 1447.
[10] M.J. Baldwin, et al., Nucl. Fusion 51 (2011), 103021.
[11] M. Yajima, et al., J. Nucl. Mater. 438 (2013) S1142.
[12] S. Kajita, et al., Nucl. Fusion 54 (2014), 033005.
[13] O.V. Ogorodnikova, et al., J. Nucl. Mater. 515 (2019) 150.
[14] S. Takamura, et al., Plasma Fusion Res. 5 (2010) 39.
[15] W. Sakaguchi, et al., J. Nucl. Mater. 390 (2009) 1149.
[16] M. Tokitani, et al., Nucl. Fusion 51 (2011), 102001.
[17] M. Yajima, et al., Fusion Eng. Des. 112 (2016) 156.
[18] J. Matějíček, et al., J. Nucl. Mater. 492 (2017) 204.
[19] D. Hwangbo, et al., Contrib. Plasma Phys. 58 (2018) 608.
[20] M.J. Baldwin, et al., J. Nucl. Mater. 390 (2009) 886.
[21] K.D. Hammond, Mater. Res. Express 4 (2017), 104002.

[22] A. Lasa, et al., EPL 105 (2014) 25002.
[23] K. Doi, et al., Fusion Eng. Des. 136 (2018) 100.
[24] K. Doi, et al., IEEE Trans. Plasma Sci. 46 (2018) 482.
[25] D.H. Liu, et al., Nucl. Fusion 60 (2020), 056018.
[26] S. Kajita, et al., J. Nucl. Mater. 421 (2012) 22.
[27] S. Kajita, et al., J. Nucl. Mater. 440 (2013) 55.
[28] D.G. Temmerman, et al., Nucl. Mater. Energy 19 (2019) 255.
[29] M. Yajima, et al., J. Nucl. Mater. 449 (2014) 9.
[30] S.Y. Dai, et al., Plasma Phys. Control Fusion 55 (2013) 55004.
[31] S.Y. Dai, et al., Nucl. Fusion 54 (2014), 123015.
[32] S.Y. Dai, et al., J. Nucl. Mater. 463 (2015) 372.
[33] Q. Shi, et al., Fusion Eng. Des. 136 (2018) 554.
[34] S.Y. Dai, et al., Nucl. Fusion 55 (2015), 043003.
[35] S.Y. Dai, et al., Nucl. Fusion 58 (2018), 014006.
[36] S.Y. Dai, et al., Nucl. Fusion 60 (2020), 026006.
[37] Y. Yamamura, et al., Radiat. Eff. 71 (1983) 65.
[38] W. Eckstein, Vacuum 82 (2008) 930.